PHYSICAL REVIEW D **74,** 035002 (2006)

Little Higgs dark matter

Andreas Birkedal,[1] Andrew Noble,[2] Maxim Perelstein,[2] and Andrew Spray[2]
[1]*SCIPP, University of California, Santa Cruz, California 95064, USA*
[2]*Cornell Institute for High-Energy Phenomenology, Cornell University, Ithaca, New York 14853, USA*
(Received 31 March 2006; published 1 August 2006)

The introduction of T parity dramatically improves the consistency of little Higgs models with precision electroweak data, and renders the lightest T-odd particle (LTP) stable. In the littlest Higgs model with T parity, the LTP is typically the T-odd heavy photon, which is weakly interacting and can play the role of dark matter. We analyze the relic abundance of the heavy photon, including its coannihilations with other T-odd particles, and map out the regions of the parameter space where it can account for the observed dark matter. We evaluate the prospects for direct and indirect discovery of the heavy photon dark matter. The direct detection rates are quite low and a substantial improvement in experimental sensitivity would be required for observation. A substantial flux of energetic gamma rays is produced in the annihilation of the heavy photons in the galactic halo. This flux can be observed by the GLAST telescope, and, if the distribution of dark matter in the halo is favorable, by ground-based telescope arrays such as VERITAS and HESS.

DOI: 10.1103/PhysRevD.74.035002 PACS numbers: 12.60.Cn, 95.35.+d

I. INTRODUCTION

It has now been firmly established that about 25% of the energy density in the universe exists in the form of nonrelativistic, nonbaryonic, nonluminous matter, so called ''dark matter'' [1]. The microscopic composition of dark matter remains a mystery, but it is clear that it cannot consist of any elementary particles that have been directly observed in the laboratory so far.[1] Many theories which extend the standard model (SM) of electroweak interactions contain new particles with the right properties to play the role of dark matter; perhaps the best known example is the lightest neutralino of supersymmetric (SUSY) models.

Recently, a new class of theories extending the SM at the TeV scale, ''Little Higgs'' (LH) models, has been proposed [2] (for reviews, see [3,4]). The LH models contain a light (possibly composite) Higgs boson, as well as additional gauge bosons, fermions, and scalar particles at the TeV scale. The Higgs is a pseudo-Nambu-Goldstone boson, corresponding to a global symmetry spontaneously broken at a scale $f \sim 1$ TeV. The global symmetry is also broken explicitly by the gauge and Yukawa couplings of the Higgs. As a result of this breaking, the Higgs acquires a potential; however, the leading (one-loop, quadratically divergent) contribution to this potential vanishes due to the special ''collective'' nature of the explicit global symmetry breaking, and the lightness of the Higgs can be achieved without fine-tuning. The dynamics of the Higgs and other degrees of freedom relevant at the TeV scale is described by a nonlinear sigma model (nlsm), valid up to the cutoff scale $\Lambda \sim 4\pi f \sim 10$ TeV.[2] In particular, the Higgs mass term is dominated by a one-loop, logarithmically enhanced contribution from the top sector, which can be computed within the nlsm and shown to have the correct sign to trigger electroweak symmetry breaking, providing a simple and attractive explanation of this phenomenon. Above the cutoff scale, the model needs to be embedded in a more fundamental theory; however, for many phenomenological applications, including the analysis of this paper, the details of that theory are not relevant and the nlsm description suffices.

The Littlest Higgs model [2] is simple and economical, and it has been the focus of most phenomenological analyses to date [6]. Unfortunately, the model suffers from severe constraints from precision electroweak fits, due to the large corrections to low-energy observables from the tree-level exchanges of the non-SM TeV-scale gauge bosons and the small but nonvanishing weak-triplet Higgs vacuum expectation value (vev) [7]. To alleviate this difficulty, the symmetry of the theory can be enhanced to include a Z_2 discrete symmetry, named ''T parity'' [8]. In the Littlest Higgs model with T parity (LHT) [9], the non-SM gauge bosons and the triplet Higgs are T-odd, forbidding all tree-level corrections to precision electroweak observables.[3] Loop corrections to precision electroweak observables in the LHT model were considered in [10], and the model was shown to give acceptable electro-

[1]In principle, it remains possible that dark matter consists of microscopic black holes made out of ordinary particles. However, we do not know of a compelling cosmological scenario in which this possibility is realized.

[2]The actual cutoff scale is model-dependent:, for example, in the Littlest Higgs model the ratio Λ/f is somewhat lower than the naive estimate of 4π, due to the large number of fields [5].

[3]In the version of the model considered here, there is one non-SM T-even state, the ''heavy top'' T_+. However it only contributes at tree level to observables involving the weak interactions of the top quark, which are at present unconstrained.

weak fits in large regions of parameter space compatible with naturalness.

An interesting side effect of T parity is that the lightest T-odd particle (LTP) is guaranteed to be stable. Analyzing the spectrum of the model, Hubisz and Meade [11] have argued that the LTP is likely to be the electricaly neutral, weakly interacting ''heavy photon'' (or, more precisely, the T-odd partner of the hypercharge gauge boson) B_H. This particle is an attractive dark matter candidate, and initial calculations [11] showed that its relic abundance is within the observed range for reasonable choices of model parameters.[4] In this paper, we will present a somewhat more detailed relic density calculation, including the possibility of coannihilations between the B_H and other T-odd particles. We will then discuss the prospects for direct and indirect detection of the heavy photon dark matter.

II. THE MODEL

Our analysis will be performed within the framework of the Littlest Higgs model with T parity, which has recently been studied in Refs. [10,11]. Let us briefly sketch the salient features of the model relevant here; for more details, see [10,11] or the review article [4].

The model is based on an $SU(5)/SO(5)$ global symmetry breaking pattern; the Higgs doublet of the SM is identified with a subset of the Goldstone boson fields associated with this breaking. The symmetry breaking occurs at a scale $f \sim 1$ TeV. An $[SU(2) \times U(1)]^2$ subgroup of the $SU(5)$ is gauged; this is broken at the scale f down to the diagonal subgroup, $SU(2)_L \times U(1)_Y$, identified with the SM electroweak gauge group. The extended gauge structure results in four additional gauge bosons at the TeV scale, $W_H^{\pm}$, W_H^3, and B_H.[5]

T parity is an automorphism which exchanges the $[SU(2) \times U(1)]_1$ and $[SU(2) \times U(1)]_2$ gauge fields; under this transformation, the TeV-scale gauge bosons are odd, whereas the SM gauge bosons are even. The odd gauge bosons have masses

$$M(W_H^a) \approx gf, \qquad M \equiv M(B_H) \approx \frac{g'f}{\sqrt{5}} \approx 0.16f, \quad (1)$$

where g and g' are the SM $SU(2)_L$ and $U(1)_Y$ gauge couplings, and the normalization of f is the same as in Ref. [10]. (Electroweak symmetry breaking at the scale $v \ll f$ induces corrections to these formulas of order v^2/f^2.) The ''heavy photon'' B_H is the lightest new gauge boson, and in fact is quite light compared to f. Since the masses of the other T-odd particles are generically of order f, we will assume that the B_H is the lightest T-odd particle (LTP), and it will play the role of dark matter candidate. The only direct coupling of the heavy photon to the SM sector is via the Higgs, resulting in weak-strength cross sections for B_H scattering into SM states. The heavy photon then provides yet another explicit example of a weakly interacting massive particle (WIMP) dark matter candidate, and it is not surprising that we will find reasonable regions of parameter space where it can account for all of the observed dark matter. For later convenience, we denote the mass of this particle by M. The range of the allowed values for this parameter is determined by the precision electroweak constraints, which put a lower bound on f, typically of about 600 GeV [10]. While there is no firm upper bound on f, we will assume $f \lesssim 2$ TeV to avoid reintroducing fine-tuning in the Higgs sector. Using Eq. (1), this corresponds to a WIMP mass in the range

$$100 \text{ GeV} \lesssim M \lesssim 300 \text{ GeV}. \quad (2)$$

In the scalar sector, the model contains an additional T-odd weak-triplet field ϕ, which has a mass of order f and no vacuum expectation value. In the fermion sector, each SM doublet (Q_i^a and L_i, where $a = 1 \ldots 3$ is a color index and $i = 1 \ldots 3$ is a generation index), acquires a T-odd partner, $\tilde{Q}_i^a$ and $\tilde{L}_i$. The masses of these particles are also free parameters,[6] with the natural scale set by f. To avoid proliferation of parameters, we will assume a universal T-odd fermion mass $\tilde{M}$ for both lepton and quark partners; we will require $\tilde{M} > M$ to avoid charged or colored LTPs, and assume $\tilde{M} \gtrsim 300$ GeV, since otherwise the colored T-odd particles would have been detected in squark searches at the Tevatron. In addition, nonobservation of four-fermion operator corrections to SM processes such as $e^+e^- \to q\bar{q}$ places an *upper* bound on the T-odd fermion masses [10]:

$$\tilde{M}_{\text{TeV}} < 4.8 f_{\text{TeV}}^2, \quad (3)$$

where $\tilde{M}$ and f are expressed in units of TeV. To cancel the one-loop quadratic divergence in the Higgs mass due to top loops, two additional new fermions are required in the top sector, the T-even T_+ and the T-odd T_-.[7] Their masses are related by

[4]While the LHT dark matter candidate is a spin-1 heavy photon, this is not an unambiguous prediction of Little Higgs models. For example, the ''simplest little Higgs'' models [12] supplemented by T-parity may contain a stable heavy neutrino which can play the role of dark matter [13], while closely related ''theory space'' models can give rise to a scalar WIMP dark matter candidate [14].

[5]The W_H^3 and B_H fields mix to form the two neutral mass eigenstates; however, the mixing angle is of order v/f and can typically be neglected.

[6]If the flavor structure of the T-odd quark mass matrix is generic, with order-one flavor mixing angles, the masses of the T-odd quarks need to be degenerate at the few per cent level [15].

[7]In Ref. [16], a variation of the model has been constructed where a single T-odd top partner is sufficient to cancel the divergences. Since the top sector will only play a minor role in the analysis of this paper, we expect our results to hold, at least qualitatively, in that model.

TABLE I. Interaction vertices involving the heavy photon B_H that appear in the calculations of this paper. Here $\alpha = \cos^{-1}(M_{T_-}/M_{T_+})$, and $\tilde{Y} = 1/10$.

$B_H^\mu B_H^\nu h$	$-\frac{i}{2} g'^2 v g^{\mu\nu}$
$B_H^\mu B_H^\nu hh$	$-\frac{i}{2} g'^2 g^{\mu\nu}$
$B_H^\mu \tilde{Q}_i^a Q_j^b$	$i\tilde{Y} g' \gamma^\mu P_L \delta_{ij} \delta^{ab}$
$B_H^\mu \tilde{L}_i L_i$	$i\tilde{Y} g' \gamma^\mu P_L \delta_{ij}$
$B_H^\mu T_- t$	$i(\frac{2}{5}) g' \gamma^\mu \sin\alpha (\sin\alpha \frac{v}{f} P_L + P_R)$

$$M_{T_+} = M_{T_-}\left(1 - \frac{m_t^2 f^2}{v^2 M_{T_-}^2}\right)^{-1/2}, \tag{4}$$

so that there is just one additional independent parameter in this sector. We will choose it to be M_{T_-}, and assume $M_{T_-} > M$ to avoid a charged LTP. The couplings of the heavy photon B_H which will be used in the calculations of this paper are summarized in Table I. Note that the embedding of the heavy photon and the standard model Z in the gauge group of the model implies that the trilinear $B_H B_H Z$ coupling vanishes at any level in the v/f expansion. (This is in contrast to the case of the supersymmetric neutralino, which acquires a $\chi_1^0 \chi_1^0 Z$ coupling due to its higgsino component.)

III. RELIC DENSITY CALCULATION

In the early universe, the heavy photons are in equilibrium with the rest of the cosmic fluid. In the simplest case of a generic (nondegenerate) T-odd particle mass spectrum, the equilibrium is maintained via the heavy photon pair-annihilation and pair-creation reactions; the leading $2 \leftrightarrow 2$ processes that contribute are shown in Fig. 1. The present relic abundance of heavy photons is determined by the behavior of pair-annihilation rates in the nonrelativistic limit, namely, by the sum of the quantities

$$a(X) = \lim_{u \to 0} \sigma(B_H B_H \to X) u, \tag{5}$$

over all possible final states X. Here, u is the relative velocity of the annihilating particles. Note that, unlike the binolike neutralinos typically predicted by the constrained minimal supersymmetric standard model (cMSSM), the s-wave annihilation of the heavy photons is unsuppressed: in the language of Ref. [17], the heavy photons are "s annihilators", analogous to the Kaluza-Klein photons of the "universal extra dimensions" (UED) model [18,19]. It is straightforward to compute $a(X)$ using the Feynman rules in Table I. We obtain

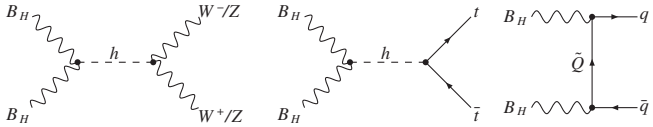

FIG. 1. The leading $2 \leftrightarrow 2$ processes which maintain the heavy photon in equilibrium with the rest of the cosmic fluid at high temperatures.

$$\begin{aligned} a(W^+W^-) &= \frac{2\pi\alpha^2}{3\cos^4\theta_W} \frac{M^2}{(4M^2 - m_h^2)^2 + m_h^2\Gamma_h^2} \\ &\quad \times \left(1 - \mu_w + \frac{3}{4}\mu_w^2\right)\sqrt{1-\mu_w}, \\ a(ZZ) &= \frac{\pi\alpha^2}{3\cos^4\theta_W} \frac{M^2}{(4M^2 - m_h^2)^2 + m_h^2\Gamma_h^2} \\ &\quad \times \left(1 - \mu_z + \frac{3}{4}\mu_z^2\right)\sqrt{1-\mu_z}, \end{aligned} \tag{6}$$

where $\mu_i = m_i^2/M^2$, θ_W is the SM weak mixing angle, and m_h and Γ_h are the mass and the width of the SM Higgs boson. If $M > m_t$, the LTPs can also annihilate into pairs of top quarks; ignoring the contribution from the t- and u-channel T_- exchanges, we obtain[8]

$$a(t\bar{t}) = \frac{\pi\alpha^2}{4\cos^4\theta_W} \frac{M^2}{(4M^2 - m_h^2)^2 + m_h^2\Gamma_h^2} \mu_t (1 - \mu_t)^{3/2}. \tag{7}$$

If $M > m_h$, annihilation into a pair of Higgs bosons is possible, with the cross section

$$\begin{aligned} a(hh) &= \frac{\pi\alpha^2 M^2}{2\cos^4\theta_W}\left[\frac{\mu_h(1 + \mu_h/8)}{(4M^2 - m_h^2)^2 + m_h^2\Gamma_h^2} + \frac{1}{24M^4}\right] \\ &\quad \times \sqrt{1-\mu_h}. \end{aligned} \tag{8}$$

Finally, LTPs can also annihilate into light SM fermions via t-channel exchanges of the T-odd fermions; this channel was not included in the analysis of Ref. [11]. For a fermion f ($f = \ell^\pm, \nu, u, d$) we obtain

$$a(f\bar{f}) = \frac{16\pi\alpha^2 \tilde{Y}^4 N_c^f}{9\cos^4\theta_W} \frac{M^2}{(M^2 + \tilde{M}^2)^2}, \tag{9}$$

where $N_c^f = 1$ for leptons and 3 for quarks, and $\tilde{Y} = 1/10$ is the $B_H f \tilde{f}$ coupling in units of g'. Because of the small value of $\tilde{Y}$, the annihilation into light fermions is strongly suppressed, even for relatively small values of $\tilde{M}$. The WMAP collaboration data [20] provides a precise determination of the present dark matter abundance: at the two-sigma level,

[8]The T_- exchanges are negligible throughout most of the parameter space, but will nevertheless be fully included in the numerical calculation of the relic abundance described below.

$$\Omega_{\rm dm}h^2 = 0.111 \pm 0.018. \qquad (10)$$

For s annihilators, this translates into a determination of the quantity $a \equiv \sum_X a(X)$: $a = 0.8 \pm 0.1$ pb. (The precise central value of a depends on the WIMP mass; however, this dependence is very mild, see Fig. 1 of Ref. [17].) Using this constraint and the above formulas, it is straightforward to map out the regions of the model parameter space where the heavy photons can account for all of the observed dark matter. The results are consistent with the updated analysis of Hubisz and Meade, see Fig. 3 of Ref. [11]. For given m_h, there are two values of M which result in the correct relic density. There is one solution on either side of the Higgs resonance. For WIMP masses in the interesting range, Eq. (2), these can be approximated by simple analytic expressions:

$$m_h \approx 24 + 2.38M \quad \text{or} \quad m_h \approx -83 + 1.89M, \qquad (11)$$

where M and m_h are in units of GeV. We will refer to these solutions as ''low'' and ''high'', respectively. The analytic expressions (11) reproduce the values of M and m_h consistent with the WMAP central value of $\Omega_{\rm dm}h^2$ with an error of at most a few GeV throughout the interesting parameter range. This accuracy will be sufficient for the analysis of detection prospects in Secs. IV and V.

Throughout the parameter space consistent with the WMAP value of the present dark matter density, the dominant heavy photon annihilation channels are W^+W^- and ZZ; the $t\bar{t}$ channel contributes at most about 5% of the total annihilation cross section, while the hh final state is always kinematically forbidden. Moreover, the ratio of the W^+W^- and ZZ contributions is approximately 2:1, as is evident from Eqs. (6), so that $a(W^+W^-) \approx 0.53$ pb, $a(ZZ) \approx 0.27$ pb throughout the parameter space. Since B_H is an s-annihilator, the same cross sections govern the rate of heavy photon annihilation in the galactic halo, which in turn determines the fluxes relevant for indirect detection, see Sec. V.

If some of the T-odd particles are approximately degenerate in mass with the heavy photon, the simple analysis above is no longer applicable, since coannihilation reactions between B_H and other states significantly affect the relic abundance. In the LHT model, the masses of the T-odd weak gauge bosons W_H and the triplet scalar ϕ are predicted unambiguously once the scale f and the Higgs mass m_h are fixed; these particles are always much heavier than the B_H and their effect is negligible. On the other hand, the common mass scale of the T-odd leptons and quarks $\tilde{M}$ is a free parameter, and for $M \sim \tilde{M}$ the coannihilations between these states and the B_H can be important. We have performed a more detailed analysis of the B_H relic density, taking this possibility into account.

In the presence of coannihilations, the abundance calculation requires solving a system of coupled Boltzmann equations. We approached this problem numerically. The interactions of the LHT model were incorporated in the CALCHEP package [21], which was used to compute the scattering matrix elements for the appropriate processes. The rest of the calculation was performed using the DM++ package,[9] recently developed by one of us (AB). The package first uses the matrix elements to compute the thermal averages $\langle \sigma u \rangle$, which determine the reaction rates entering the Boltzmann equation. Then, the freeze-out temperature of the dark matter is determined iteratively, using the Turner-Scherrer approximation [25]. Finally, the integral of $\langle \sigma u \rangle$ from freeze-out to present day (usually called $J(x_F)$ in the literature) is evaluated, providing the relic abundance.

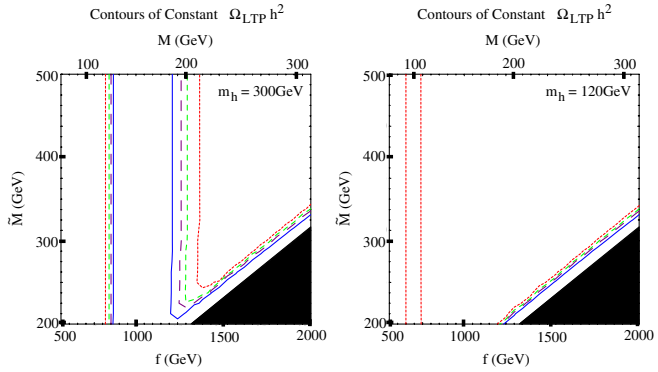

FIG. 2 (color online). The contours of constant present abundance of the heavy photon LTP, $\Omega_{\rm LTP}h^2$, in the M-$\tilde{M}$ plane. The Higgs mass is taken to be 300 GeV (left panel) and 120 GeV (right panel). The red (dotted) and green (short-dashed) contours correspond to the upper and lower bounds from WMAP, Eq. (10), assuming that the LTP makes up all of dark matter. The purple (long-dashed) and blue (solid) lines correspond to the LTP contributing 50% and 70%, respectively, of the measured dark matter density. The shaded region corresponds to a charged and/or colored LTP.

The results of this analysis are illustrated by Fig. 2, which shows the contours of constant heavy photon relic density in the $f - \tilde{M}$ (or, equivalently, $M - \tilde{M}$) plane. The typical situation for a heavy Higgs is shown in the left panel ($m_h = 300$ GeV). There are two regions in which the heavy photon can account for the observed dark matter:

(i) The two vertical *pair-annihilation bands*, where the coannihilation processes are unimportant. The heavy photon abundance in these regions is independent of $\tilde{M}$. The bands appear on either side of the s-channel Higgs resonance dominating the pair-annihilation processes, corresponding to the high and low solutions of Eq. (11). (The bands are analogous to the ''Higgs funnel'' region in the cMSSM.)

[9]The DM++ is inspired by the MICROMEGAS code [22], which was originally designed to compute the relic abundance of neutralinos in the MSSM. The recently developed new version of this code, MICROMEGAS 2.0 [23], is also applicable to any CALCHEP model defined by the user. This package is now publicly available [24].

(ii) The *coannihilation tail*, where the heavy photon abundance is predominantly set by coannihilation processes. Since the T-odd fermions are assumed to be degenerate, all of them participate in the coannihilation reactions. The location and shape of this feature are similar to the stau coannihilation tail in cMSSM.

As the Higgs mass is decreased, the pair-annihilation bands appear for lower WIMP masses, and for light Higgs (115–150 GeV) the low band disappears, since the required values of f are already ruled out by data. The high band persists until the Higgs mass is close to the current experimental bound. To illustrate this, consider the right panel of Fig. 2, where $m_h = 120$ GeV. The band between the two red lines ($90 \lesssim M \lesssim 100$ GeV) is allowed. Note that the behavior of the relic density as a function of M within this band is nontrivial: The relic density first drops with increasing M due to the fact that the threshold for the reaction $B_H B_H \to ZZ$ is passed. It then bottoms out at a value consistent with the measured $\Omega_{\rm dm} h^2$, and begins increasing as increasing M further takes the center-of-mass energy away from the Higgs resonance, suppressing annihilation. Clearly, this situation is quite nongeneric, and for somewhat higher m_h the Z threshold becomes irrelevant and relic density is a uniformly increasing function of M in the high band. The coannihilation tail is present for low as well as high values of m_h. The tail can be described by a simple analytic formula

$$\tilde{M} \approx M + 20 \text{ GeV}, \tag{12}$$

which is approximately independent of the Higgs mass.

It should be noted that the remaining free parameter of our model, the mass of the second T-odd top quark M_{T_-}, was fixed to be equal to f, so that $M_{T_-} \gg M$ and this particle did not have an effect on the B_H relic abundance. We expect that a second coannihilation tail appears when $M_{T_-} \sim M$; the structure should be very similar to the one found above, with slight numerical differences due to the smaller multiplicity of coannihilating states.

IV. DIRECT DETECTION

Direct dark matter detection experiments attempt to observe the recoil energy transfered to a target nucleus in an elastic collision with a WIMP. The null result of the current experiments places an upper bound on the cross section of elastic WIMP-nucleon scattering. In this section, we will discuss the implications of this bound for the LHT dark matter, and prospects for future discovery.

The elastic scattering of the heavy photon on a nucleus receives contributions from several processes shown in Fig. 3. Consider first the scattering off gluons, which occurs via the Higgs exchange diagram (a). The Higgs-gluon coupling arises predominantly via a top quark loop, and has the form [26]

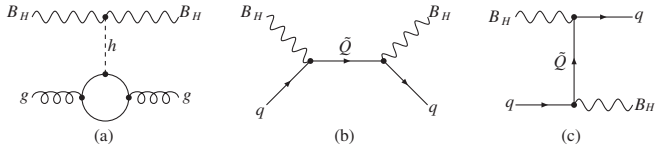

FIG. 3. The leading processes which contribute to the heavy photon-nucleon elastic scattering cross section relevant for direct dark matter detection experiments.

$$\mathcal{L}_{hgg} = \frac{\alpha_s}{12\pi v} h G^a_{\mu\nu} G^{a\mu\nu}. \tag{13}$$

where $v = 246$ GeV is the Higgs vev, and $G^a_{\mu\nu}$ is the color field strength. The halo WIMPs are highly nonrelativistic ($\beta \sim 10^{-3}$), and the momentum transfer in the reaction at hand is negligible compared to m_h. The WIMP-gluon interaction can then be described by an effective operator

$$\frac{\alpha_s \alpha}{6\cos^2\theta_W} \frac{1}{m_h^2} B_{H\alpha} B_H^\alpha G^a_{\mu\nu} G^{a\mu\nu}. \tag{14}$$

In the chiral limit, the matrix element $\langle n|G^2|n\rangle$ can be related to the nucleon mass m_n [26], leading to an effective WIMP-nucleon vertex of the form

$$\mathcal{L}_{\rm eff} = \frac{e^2}{27\cos^2\theta_W} \frac{m_n}{m_h^2} B_{H\alpha} B_H^\alpha \bar{\Psi}_n \Psi_n, \tag{15}$$

where Ψ_n is the nucleon (neutron or proton) field. It is clear that this interaction only contributes to the spin-independent (SI) part of the WIMP-nucleon scattering cross section. Neglecting other contributions to the SI cross section (which, as we will argue below, are expected to be subdominant), we obtain

$$\sigma_{\rm SI} = \frac{4\pi\alpha^2}{729\cos^4\theta_W} \frac{m_n^4}{m_h^4} \frac{1}{(M + m_n)^2}, \tag{16}$$

for both neutrons and protons. Since the scattering off nucleons in a given nucleus is coherent and the matrix elements for neutrons and protons are identical, the SI cross section for scattering off a nucleus of mass m_N is simply obtained from Eq. (16) by a substitution $m_n \to m_N$.

The interaction of WIMPs with quarks is dominated by the T-odd quark exchange diagrams, see Fig. 3(b) and 3(c). (The Higgs exchange diagrams are suppressed due to small Yukawa couplings of quarks. In fact, it is well known that the Higgs-nucleon interaction is dominated by the Higgs-gluon coupling considered above.) The scattering amplitude is given by

$$-i \frac{e^2 \tilde{Y}^2}{\cos^2\theta_W} \varepsilon^*_\mu(p_3) \varepsilon_\nu(p_1) \bar{u}(p_4) \left[\frac{\gamma^\mu \not{k}_1 \gamma^\nu}{k_1^2 - \tilde{M}^2} + \frac{\gamma^\nu \not{k}_2 \gamma^\mu}{k_2^2 - \tilde{M}^2} \right] \times P_L u(p_2), \tag{17}$$

where $k_1 = p_1 + p_2, k_2 = p_2 - p_3$. The $q\tilde{q}B_H$ coupling is flavor-independent, $\tilde{Y} = 1/10$, and the expression (17) is valid for every quark species. The amplitude contains two

important physical scales: the weak scale, $M \sim \tilde{M} \sim 100$ GeV, and the QCD scale, $\Lambda_{\rm QCD} \sim 100$ MeV, which represents the typical energy and momentum of the quarks bound inside a stationary nucleus and, by a coincidence, the spatial momenta of the halo WIMPs: $|\mathbf{p}|_{1,3} \sim \beta M \sim \Lambda_{\rm QCD}$. We will work to leading order in the ratio of these two scales. In this approximation, $k_1 \approx -k_2 \approx (M, \mathbf{0})$, and the heavy photon polarization vectors are purely spatial, $\varepsilon^\mu(p_{1,3}) = (0, \varepsilon_{1,3})$. The amplitude takes the form

$$\frac{e^2\tilde{Y}^2}{\cos^2\theta_W}\frac{M}{M^2-\tilde{M}^2}\epsilon_{ijk}\varepsilon_1^i\varepsilon_3^j\bar{u}_4\gamma^k(1-\gamma^5)u_2, \tag{18}$$

corresponding to the coupling of the B_H spin with the vector and axial-vector quark currents. The axial current interaction corresponds to the coupling between the WIMP and quark spins, and gives rise to the spin-dependent (SD) part of the WIMP-nucleus scattering cross section. By the Wigner-Eckardt theorem, the quark axial current can be replaced by the nuclear spin operator s_N^μ:

$$\langle N|\bar{q}\gamma^\mu\gamma^5 q|N\rangle = 2s_N^\mu\lambda_q. \tag{19}$$

For a nucleus of spin J_N, the coefficients are given by

$$\lambda_q = \Delta q_p\frac{\langle S_p\rangle}{J_N} + \Delta q_n\frac{\langle S_n\rangle}{J_N}, \tag{20}$$

where $\langle S_{p,n}\rangle/J_N$ is the fraction of the total nuclear spin carried by protons and neutrons, respectively, and the quantities Δq_n can be extracted from deep inelastic scattering data. We will use $\Delta u_p = \Delta d_n = 0.78 \pm 0.02$, $\Delta d_p = \Delta u_n = -0.48 \pm 0.02$, $\Delta s_n = \Delta s_p = -0.15 \pm 0.02$ [27]. The effective WIMP-nucleus spin-spin interaction can then be written as

$$\frac{2e^2\tilde{Y}^2M}{\cos^2\theta_W(M^2-\tilde{M}^2)}\epsilon_{ijk}B_H^iB_H^j\bar{\Psi}_N s_N^k\Psi_N\sum_{q=u,d,s}\lambda_q, \tag{21}$$

yielding the SD cross section

$$\sigma_{\rm SD} = \frac{16\pi\alpha^2\tilde{Y}^4}{3\cos^4\theta_W}\frac{m_N^2}{(M+m_N)^2}\frac{M^2}{(M^2-\tilde{M}^2)^2}J_N(J_N+1) \times\left(\sum_{q=u,d,s}\lambda_q\right)^2. \tag{22}$$

Now, consider the part of the amplitude (18) involving the quark vector current. Since the current is conserved, the contributions of each valence quark in a nucleon add coherently, and sea quarks do not contribute. The resulting WIMP-nucleon coupling is

$$\frac{3e^2\tilde{Y}^2M}{\cos^2\theta_W(M^2-\tilde{M}^2)}\epsilon_{ijk}B_H^iB_H^j\bar{\Psi}_n\gamma^k\Psi_n. \tag{23}$$

This interaction is suppressed in the nonrelativistic limit, since $\bar{u}_n\gamma^k u_n \sim v_n^k$. In fact, it is of the same order as other contributions to the WIMP-quark scattering amplitude, suppressed by WIMP velocities or powers of $\Lambda_{\rm QCD}/M$, which were neglected in our analysis. Therefore, its effect will be neglected.

It should be noted that the SI interaction in Eq. (15) is parametrically suppressed with respect to the leading SD coupling, Eq. (21), by a factor of $m_N/m_h \sim \Lambda_{\rm QCD}/M$, and is formally of the same order as the contributions to the WIMP-quark interaction that were neglected in our analysis. Since the neglected terms contribute to the SI as well as SD interactions, one may question the validity of the SI cross section obtained in Eq. (16). Note, however, that the WIMP-quark interactions are additionally suppressed by a factor of $\tilde{Y}^2 = 0.01$, not present in the WIMP-gluon couplings. Thus, while of the same order as (15) in terms of power counting, the neglected SI corrections from WIMP-quark interactions are expected to be numerically small. One interesting potential exception occurs in the coannihilation region, where the $\tilde{Y}$ suppression could be compensated by the factor of $\tilde{M} - M \ll M$ in the propagator, and the WIMP-quark interactions could provide a significant correction to Eq. (16). A detailed analysis of this issue is reserved for future study.

The SI elastic WIMP-nucleon scattering cross sections expected in the LHT models are plotted in Fig. 4, along with the current bound from the CDMS collaboration [28] (solid red lines) and the projected future sensitivity of SuperCDMS, Stage C [29] (dashed red lines). We assume that the heavy photons account for all of the observed dark matter, and the two panels correspond to the two regions of parameter space which satisfy this constraint. The left panel shows the cross section expected in the pair-annihilation bands, with the two lines corresponding to the high and low solutions in Eq. (11). The right panel shows the cross section expected in the coannihilation tail for two values of the Higgs mass, 120 GeV and 300 GeV.

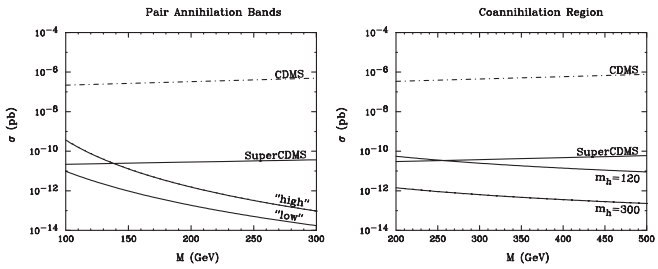

FIG. 4. The spin-independent (SI) WIMP-nucleon elastic scattering cross section in the pair-annihilation bands (left panel) and in the coannihilation region, for two values of m_h, 120 and 300 GeV (right panel). The present [28] and projected [29] sensitivities of the CDMS experiment are also shown.

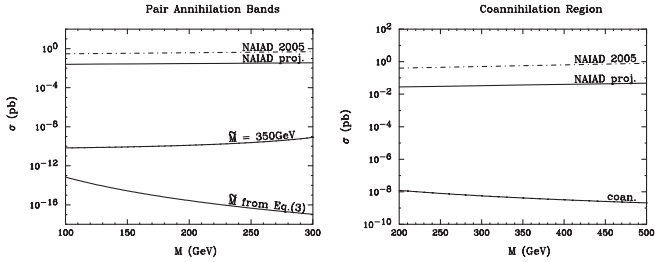

FIG. 5. The spin-dependent (SD) WIMP-proton elastic scattering cross section in the pair-annihilation bands (left panel) and in the coannihilation region (right panel). In the pair-annihilation bands, the scale $\tilde{M}$ is allowed to vary between 350 GeV and the upper bound given in Eq. (3). The present [30] and projected [31] sensitivities of the NAIAD experiment are also shown.

The two lines can be thought of as the upper and lower bounds on the expected cross section.[10] While the predicted cross sections are two-to-3 orders of magnitude below the present sensitivity, the expected improvements of the CDMS experiments will allow it to begin probing the interesting regions of the model parameter space in both pair-annihilation and coannihilation regions.

Figure 5 shows the spin-dependent cross sections predicted by the LHT model, along with the current bound from the NAIAD experiment [30] and its projected sensitivity [31]. In the pair-annihilation bands, the scale $\tilde{M}$ is allowed to vary between 350 GeV and the upper bound given in Eq. (3). [Recall that for a given value of M, the scale f is fixed unambiguously by Eq. (1).] Unfortunately, the predicted SD cross sections are several orders of magnitude below the NAIAD sensitivity.

V. INDIRECT DETECTION VIA ANOMALOUS GAMMA RAYS

As discussed in Section III, WIMP annihilation processes have to occur with approximately weak-scale cross sections to ensure that the relic abundance of WIMPs is consistent with observations. Since the heavy photons of the LHT model are s-annihilators, their annihilation rates are approximately velocity-independent in the nonrelativistic regime. This implies that the WIMPs collected, for example, in galactic halos, have a substantial probability to pair-annihilate, resulting in anomalous high-energy cosmic rays which could be distinguished from astrophysical backgrounds. In particular, high-energy gamma rays (photons) and positrons are considered to be the most promising experimental signatures. The gamma-ray signal is particularly interesting because the gamma rays in the relevant energy range travel over galactic scales with no scattering,

[10]Note, however, that in the LHT model a heavy Higgs, $m_h >$ 300 GeV, may be consistent with precision electroweak data in certain regions of parameter space where its contribution to the T parameter is partially cancelled by new physics contributions [10]. A heavier Higgs corresponds to smaller SI cross section.

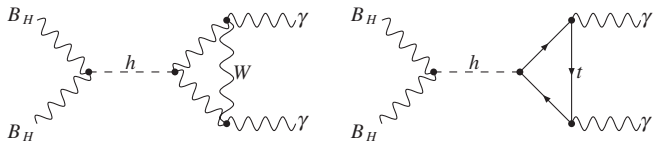

FIG. 6. The diagrams which dominate the monochromatic photon pair-production in the B_H annihilation in the galactic halo.

so that if the signal is observed, information about the WIMP (e.g. its mass) could be extracted from the spectrum. In this section, we will compute the gamma-ray fluxes predicted by the LHT model, and evaluate their observability.[11]

There are three principal mechanisms by which hard photons can be produced in WIMP annihilation:

(i) Monochromatic photons produced via direct annihilation into a two-body final state ($\gamma\gamma$, $h\gamma$ or $Z\gamma$);
(ii) Photons radiated in the process of hadronization and fragmentation of strongly interacting particles produced either directly in WIMP annihilation (e.g. $B_H B_H \to q\bar{q}$) or in hadronic decays of the primary annihilation products (e.g. $B_H B_H \to ZZ$ followed by $Z \to q\bar{q}$);
(iii) Photons produced via radiation from a final state charged particle.

Let us consider each of these mechanisms in turn in the LHT model.

WIMPs being electrically neutral, production of monochromatic photons can only occur at loop level. In this paper, we will concentrate on the $\gamma\gamma$ final state, postponing the analysis of the $Z\gamma$ and $h\gamma$ channels for future work. (The photons produced in these reactions are separated in energy from the $\gamma\gamma$ photons due to nonzero masses of the Z and the Higgs.) The $B_H B_H \to \gamma\gamma$ process is dominated by the one-loop diagrams inducing the effective $h\gamma\gamma$ vertex, see Fig. 6.[12] The corresponding cross section can be easily evaluated using the well-known formulas for the Higgs boson partial widths:

$$\sigma_{\gamma\gamma} u \equiv \sigma(B_H B_H \to \gamma\gamma) u = \frac{g'^4 v^2}{72 M^4} \frac{s^2 - 4sM^2 + 12M^4}{(s - m_h^2)^2 + m_h^2 \Gamma_h^2} \frac{\hat{\Gamma}(h \to V_1 V_2)}{\sqrt{s}}, \quad (24)$$

where u is the relative velocity of the annihilating WIMPs, and $s \approx 4M^2$ in the nonrelativistic regime relevant for the galactic WIMP annihilation. The hat on Γ indicates that the

[11]Positron fluxes from the heavy photon dark matter annihilation in the LHT model were recently considered in Ref. [32].

[12]A complete calculation would also include the contribution of the box diagrams with T-odd and T-even quarks running in the loop, analogous to the quark/squark boxes entering in the case of MSSM neutralino annihilation [33]. In the LHT case, this contribution is expected to be subdominant since the matrix element contains a factor of $\tilde{Y}^2 = 0.01$.

substitution $m_h \to \sqrt{s}$ should be performed in the standard expressions for on-shell Higgs decays [34,35], and the loops of new particles present in the LHT model should be included. We obtain

$$\hat{\Gamma}(h \to \gamma\gamma) = \frac{\alpha^2 g^2}{1024\pi^3} \frac{s^{3/2}}{m_W^2} |\mathcal{A}_1 + \mathcal{A}_{1/2} + \mathcal{A}_0|^2, \quad (25)$$

where $\mathcal{A}_s$ denotes the contribution from loops of particles of spin s. These contributions are given by

$$\begin{aligned} \mathcal{A}_1 &= \sum_i c_i Q_i^2 \frac{\tau_W}{\tau_i} F_1(\tau_i); \\ \mathcal{A}_{1/2} &= \sum_i \frac{\sqrt{2} Q_i^2 y_i}{g} \frac{\tau_W^{1/2}}{\tau_i^{1/2}} F_{1/2}(\tau_i); \\ \mathcal{A}_0 &= \sum_i \frac{2 Q_i^2 \lambda_i}{g^2} \frac{\tau_W}{\tau_i} F_0(\tau_i), \end{aligned} \quad (26)$$

where the sums run over all the charged particles of a given spin, and implicitly include summations over colors and other quantum numbers where necessary. The particles in the sums have masses m_i and electric charges (in units of the electron charge) Q_i; their trilinear couplings to the Higgs boson are given by $\lambda_i v$, $y_i/\sqrt{2}$, and $c_i g M_W \eta^{\mu\nu}$, for particles of spin 0, 1/2, and 1, respectively. (With these normalization choices, $c_i = 1$ for the SM $W^\pm$, and y_i's are the usual Yukawas for the SM fermions.) We have also defined $\tau_i = 4m_i^2/s$. The functions $F_s(\tau)$ are given by

$$\begin{aligned} F_1(\tau) &= 2 + 3\tau + 3\tau(2-\tau) f(\tau), \\ F_{1/2}(\tau) &= -2\tau(1 + (1-\tau) f(\tau)), \\ F_0(\tau) &= \tau(1 - \tau f(\tau)), \end{aligned} \quad (27)$$

where

$$\begin{aligned} f(\tau) &= \left[\sin^{-1}\left(\sqrt{\frac{1}{\tau}}\right) \right]^2 \quad \text{if } \tau > 1, \\ &-\frac{1}{4}\left[\log\left(\frac{1+\sqrt{1-\tau}}{1-\sqrt{1-\tau}}\right) - i\pi \right]^2 \quad \text{if } \tau < 1. \end{aligned} \quad (28)$$

Using these expressions, we find that the contributions of the T-odd states are subdominant compared to the SM loops. The contributions of the T-odd fermion loops and the T-even heavy top loop are suppressed because their coupling to the Higgs is of order v^2/f^2. The contributions of charged T-odd heavy gauge bosons and scalars are suppressed due to their large masses, of order f. The deviation of the effective $h\gamma\gamma$ coupling from its standard model value due to these states is of order a few per cent.[13] Given the much larger astrophysical uncertainties inherent in the anomalous photon flux predictions, we will ignore these effects in our analysis.

The monochromatic flux due to the $\gamma\gamma$ final state, observed by a telescope with a line of sight parametrized by $\Psi = (\theta, \varphi)$ and a field of view $\Delta\Omega$ can be written as [38]

$$\begin{aligned} \Phi = (1.1 \times 10^{-9}\ \mathrm{s}^{-1}\,\mathrm{cm}^{-2}) &\left(\frac{\sigma_{\gamma\gamma} u}{1\ \mathrm{pb}}\right) \\ &\times \left(\frac{100\ \mathrm{GeV}}{M}\right)^2 \bar{J}(\Psi, \Delta\Omega)\Delta\Omega. \end{aligned} \quad (29)$$

The function $\bar{J}$ contains the dependence of the flux on the halo dark matter density distribution:

$$\begin{aligned} \bar{J}(\Psi, \Delta\Omega) \equiv \frac{1}{8.5\ \mathrm{kpc}} &\left(\frac{1}{0.3\ \mathrm{GeV/cm}^3}\right)^2 \frac{1}{\Delta\Omega} \\ &\times \int_{\Delta\Omega} d\Omega \int_\Psi \rho^2 dl. \end{aligned} \quad (30)$$

where l is the distance from the observer along the line of sight. Many models of the galactic halo predict a sharp peak in the dark matter density in the neighborhood of the galactic center, making the line of sight towards the center the preferred one for WIMP searches.[14] However, the features of the predicted peak are highly model-dependent, resulting in a large uncertainty in the predicted $\bar{J}$. For example, at $\Delta\Omega = 10^{-3}$ sr, characteristic of ground-based Atmospheric Cerenkov Telescopes (ACTs), typical values of $\bar{J}$ range from 10^3 for the NFW profile [40] to about 10^5 for the profile of Moore *et al.* [41], and can be further enhanced by a factor of up to 10^2 due to the effects of adiabatic compression [42].

The monochromatic photon fluxes (assuming $\bar{J}\Delta\Omega = 1$) predicted by the LHT model in the parameter regions where the heavy photon accounts for all of the observed dark matter, are shown in Fig. 7. The left panel corresponds to the pair-annihilation bands, and the right panel to the coannihilation region. Searches for gamma rays from WIMP annihilation have to be able to distinguish them from the astrophysical background. In the case of the monochromatic photons, the signal is concentrated in a single bin (the energy uncertainty of the telescopes is about 10%, much larger than the intrinsic line width), and the background can be effectively measured in the neighboring bins and subtracted. In the relevant energy range, the flux sensitivity for ground-based Atmospheric Cherenkov Telescopes (ACTs) such as VERITAS [43] and HESS

[13]The deviations of the $h \to \gamma\gamma$ and $gg \to h$ vertices from the SM in the original Littlest Higgs and the LHT models were analyzed in Refs. [36,37], respectively.

[14]Note, however, that a powerful pointlike source of ultra high-energy gamma rays has been recently detected in the galactic center region [39]. The energy spectrum of this source, smooth and extending out to at least a few TeV, makes its interpretation in terms of WIMP annihilation unlikely. Detection of the potential gamma flux from WIMP annihilation in the same spatial region is clearly made more difficult by the presence of the source.

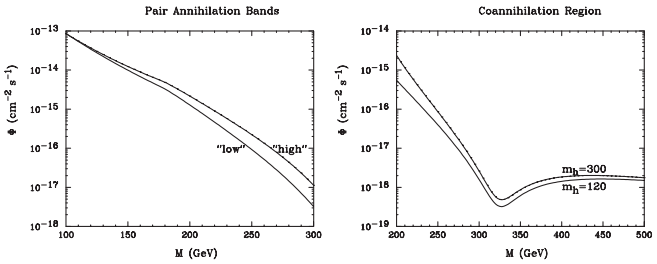

FIG. 7. The flux of the monochromatic photons from the reaction $B_H B_H \to \gamma\gamma$ in the pair-annihilation bands (left panel) and the coannihilation region (right panel). On the left panel, the upper and lower lines correspond to the high and low solutions in Eq. (11), respectively. On the right panel, the upper and lower lines correspond to $m_h = 300$ GeV and $m_h = 120$ GeV, respectively. The plots assume $\bar{J}(\Psi, \Delta\Omega)\Delta\Omega = 1$; all fluxes scale linearly with this parameter.

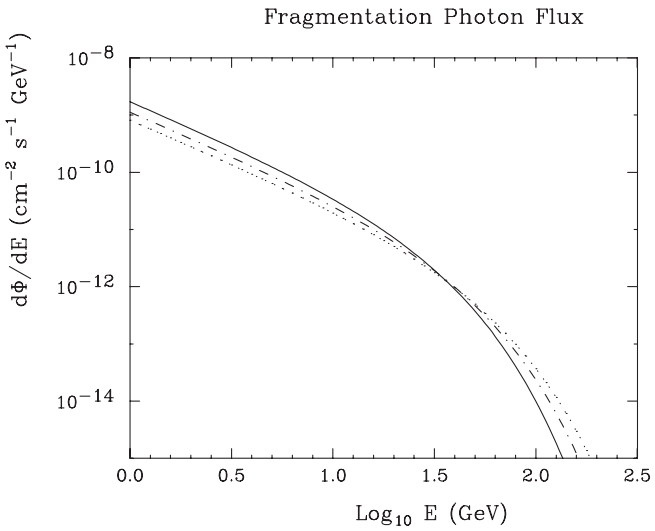

FIG. 8. The fragmentation photon flux for $M = 150$, 200, 250 GeV (solid, dot-dashed, and dotted lines, respectively), in the pair-annihilation bands. The plot assumes $\bar{J}(\Psi, \Delta\Omega)\Delta\Omega = 1$; all fluxes scale linearly with this parameter.

[44] is estimated to be around (1–5) $\times 10^{-12}$ cm^{-2} sec^{-1}, whereas the sensitivity of the upcoming space-based telescope GLAST is limited by statistics at 10^{-10} cm^{-2} sec^{-1}, assuming that 10 events are required to claim discovery [45]. It is clear that the monochromatic flux predicted by the LHT model is beyond the reach of GLAST, but could be observed at the ACTs if the dark matter distribution in the halo exhibits a substantial spike or strong clumping, $\bar{J} \gtrsim 10^5$ at $\Delta\Omega \approx 10^{-3}$.

Let us now consider the component of the photon flux due to hadronization and fragmentation of quarks produced in WIMP annihilation. As discussed in Sec. III, the heavy photons predominantly annihilate into W and Z pairs; each of the vector bosons can in turn decay into a quark pair. The resulting photon spectra depend only on the initial energies of the W's and Z's, and not on the details of the WIMP annihilation process. The spectra have been studied using PYTHIA [46] (in the MSSM context), and a simple analytic fit has been presented in Ref. [38]:

$$\frac{dN_\gamma}{dx} \approx \frac{0.73}{x^{1.5}} e^{-7.8x}. \tag{31}$$

where $x = E_\gamma/M$. This approximation is valid for both W^+W^- and ZZ final states. In the pair-annihilation bands, the differential flux is then given by

$$\frac{d\Phi}{dE} = (3.3 \times 10^{-12}\ \text{s}^{-1}\,\text{cm}^{-2}\,\text{GeV}^{-1}) \times x^{-1.5} e^{-7.8x} \left(\frac{100\ \text{GeV}}{M}\right)^3 \bar{J}(\Psi, \Delta\Omega)\Delta\Omega, \tag{32}$$

where we used the relic density constraint, $a(W^+W^-) + a(ZZ) \approx 0.8$ pb. The flux in the coannihilation region is much smaller.

The fluxes predicted by Eq. (32) for several values of M are plotted in Fig. 8. The GLAST telescope is statistics-limited at energies above about 2 GeV, and would observe tens of events in this energy range for the heavy photon mass in the preferred range, assuming $\bar{J}(\Delta\Omega)\Delta\Omega = 1$. (The flux scales linearly with this parameter combination.) One should keep in mind, however, that while the prospects for observing this signal are good, ruling out its interpretation in terms of conventional astrophysics could be challenging given the smooth, featureless nature of the fragmentation spectrum. Detailed studies of the angular distribution of these photons, in particular outside the galactic disk, will be needed.

The ACTs have a higher energy threshold, typically about 50 GeV, and suffer from an irreducible background from electron-induced showers, about 10^{-12}–10^{-10} cm^{-2} s^{-1} GeV^{-1} in the relevant energy range (50 . . . 200 GeV) for $\Delta\Omega \sim 10^{-3}$. Using the extrapolation of Ref. [38] to estimate the background, we find that the typical signal/background ratio expected at the ACTs, assuming $\Delta\Omega \sim 10^{-3}$ and $\bar{J}(\Delta\Omega)\Delta\Omega = 1$, is only about 10^{-3}. An observation of the fragmentation flux at the ACTs appears quite challenging, unless dark matter is strongly clustered at the galactic center or clumped.

The third and final component of the gamma-ray flux from WIMP annihilation is the final state radiation (FSR) photons. The FSR flux generally provides a robust signature of WIMP annihilation: it exists whenever the WIMPs have a sizable annihilation cross section into *any* charged states. The FSR photons have a continuous spectrum, in analogy to the quark fragmentation photons considered above. In fact, at low energies, the fragmentation flux dominates over the FSR component (unless WIMPs annihilate into purely leptonic states). At energies close to the WIMP mass, however, the fragmentation flux drops sharply, and the FSR component typically dominates [47]. This is particularly interesting because the FSR spec-

trum typically possesses a sharp edge feature, abruptly dropping to zero at the maximal photon energy allowed by kinematics. The edge feature could help the experiments to discern this flux on top of the (*a priori* highly uncertain) astrophysical background, and provide a measurement of the WIMP mass [47]. In the LHT model, the dominant charged two-body annihilation channel is W^+W^-, and correspondingly the reaction $B_H B_H \to W^+W^-\gamma$ provides the most important component of the FSR photon flux. The differential cross section for this process is given by

$$\frac{d\sigma}{dx}(B_H B_H \to W^+W^-\gamma) = \sigma(B_H B_H \to W^+W^-)\mathcal{F}(x;\mu_w), \tag{33}$$

where $x = 2E_\gamma/\sqrt{s} \approx E_\gamma/M$, $\mu_w = (m_W/M)^2$ and

$$\mathcal{F}(x;\mu) = \frac{\alpha}{\pi}\frac{1}{\sqrt{1-\mu}}\frac{1}{x}\times\left[(2x-2+\mu)\log\frac{2(1-x)-\mu-2\sqrt{(1-x)(1-x-\mu)}}{\mu} + 2\left(\frac{8x^2}{4-4\mu+3\mu^2}-1\right)\sqrt{(1-x)(1-x-\mu)}\right], \tag{34}$$

for $0 \le x \le 1-\mu$ and 0 for $1-\mu \le x \le 1$. In the limit of large heavy photon mass, $s \gg M_W^2$, this expression reduces to

$$\mathcal{F}(x) = \frac{2\alpha}{\pi}\frac{1-x}{x}\left[\log\frac{s(1-x)}{m_W^2} + 2x^2 - 1 + \mathcal{O}(\mu)\right]. \tag{35}$$

The leading (logarithmically enhanced) term agrees with the result obtained in Ref. [47] using the Goldstone boson equivalence theorem.[15]

The flux of the FSR photons is given by

$$\frac{d\Phi}{dE} = (5.6\times10^{-12}\ \mathrm{s^{-1}\,cm^{-2}\,GeV^{-1}}) \times\left(\frac{a(W^+W^-)}{1\ \mathrm{pb}}\right)\mathcal{F}(x;\mu_w) \times\left(\frac{100\ \mathrm{GeV}}{M}\right)^3\bar{J}(\Psi,\Delta\Omega)\Delta\Omega, \tag{36}$$

where $a(W^+W^-)$ is given in Eq. (6). Flux predictions for several representative values of M are shown in Fig. 9. In each case, the flux drops abruptly at the maximal photon energy,

$$E^\gamma_{\max} = \frac{M^2 - m_W^2}{M}. \tag{37}$$

If this edge feature were observed, it would provide a robust signature of heavy photon annihilation, as well as a measurement of its mass. Note that the FSR and fragmentation components of the flux are comparable near the edge, so that the fractional drop in the "signal" flux at the edge is significant. Just as for the monochromatic and fragmentation photons, the sensitivity to the FSR flux at ACTs is limited by the background from electron-induced showers. Assuming a 10% uncertainty on the total flux measurement, the drop in the total flux associated with the edge feature of the FSR spectrum can be observed if $\bar{J} \gtrsim 10^5$–10^6. The sensitivity at GLAST is limited by statistics, and an observation of the FSR edge requires even higher values of $\bar{J}$.

To summarize, we found that the best prospects for a discovery of anomalous gamma rays due to heavy photon annihilation in the Milky Way are offered by the GLAST telescope, which should be able to observe tens of fragmentation photons in the multi-GeV energy range. The fluxes of monochromatic and FSR photons, whose spectra

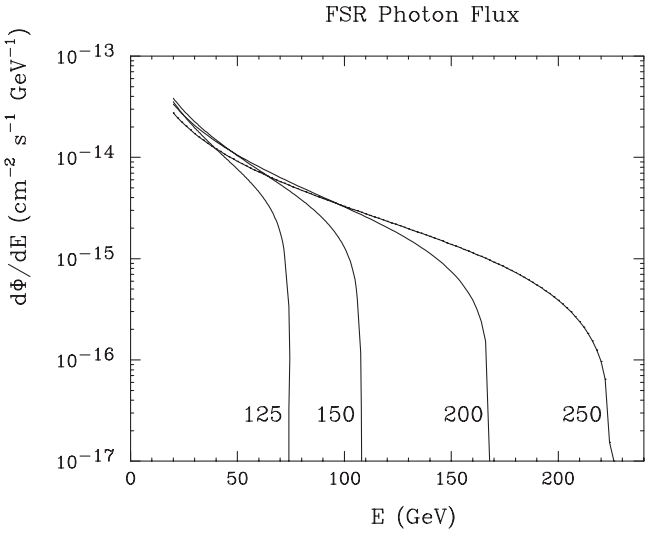

FIG. 9. The FSR photon flux for $M = 125, 150, 200, 250$ GeV (left to right), in the pair-annihilation bands. (The fluxes for high and low solutions are essentially identical.) The plot assumes $\bar{J}(\Psi,\Delta\Omega)\Delta\Omega = 1$; all fluxes scale linearly with this parameter.

[15]Note, however, that the application of the soft-collinear factorization theorem, used in the calculation of Ref. [47], to the $W^+W^-\gamma$ final state is quite subtle. For example, the $\tilde{\chi}_1^0\tilde{\chi}_1^0 \to W^+W^-\gamma$ cross section in the MSSM, computed in Ref. [48], has a different leading logarithm behavior; this is related to the fact that the W bosons effectively become massless in the large-s limit, inducing additional infrared singularities. No such singularities appear in the process considered here.

would provide clear signatures for galactic WIMP annihilation (a bump and an edge, respectively), are significantly smaller. The prospects for their detection depend on the assumed halo profile; an observation by the ACTs such as VERITAS and HESS is possible if the dark matter density has a sharp peak at the galactic center or is strongly clumped, $\bar{J} \gtrsim 10^5$–10^6.

VI. CONCLUSIONS

Little Higgs models provide an interesting alternative scenario for physics at the TeV scale, with a simple and attractive mechanism of radiative electroweak symmetry breaking. Many realistic models implementing the Little Higgs mechanism have been proposed; however, generically these models are ruled out by precision electroweak data, unless the scale f is in a few-TeV range which reintroduces fine-tuning. Little Higgs models with T parity avoid this difficulty. In this paper, we focused on the Littlest Higgs model with T parity (LHT), one of the simplest models in this class. T parity makes the lightest of the T-odd particles, the LTP, stable, enabling it to have a substantial abundance in today's universe in spite of its weak-scale mass. In the LHT model, the LTP is typically the heavy photon B_H, which can play the role of WIMP dark matter. We have computed the relic abundance of this particle, including coannihilation effects, and mapped out the regions of the parameter space where it has the correct relic abundance to account for all, or a substantial part, of the observed dark matter. These regions can be divided into the pair-annihilation bands, where the abundance is set by the B_H pair annihilation via s-channel Higgs resonance, and the coannihilation tail, where coannihilations of B_H with T-odd quarks $\tilde{Q}$ and leptons $\tilde{L}$ play the dominant role.

In the second part of the paper, we evaluated the prospects for observing the heavy photon dark matter of the LHT model using direct and indirect detection techniques. Direct detection is quite difficult, due to the fact that the heavy photon predominantly couples to the standard model states via the Higgs boson whose interactions with nucleons are weak. The elastic cross section of the B_H scattering on a nucleus in the region of parameter space consistent with the relic density constraint was found to be several orders of magnitude below the current sensitivity of direct detection searches such as CDMS. For indirect detection, we concentrated on the anomalous high-energy gamma-ray signature. The predicted gamma-ray flux depends sensitively on the distribution of dark matter in the halo. The best discovery prospect is offered by the GLAST telescope, which can observe the photons arising from the fragmentation of the W/Z bosons produced in the heavy photon annihilation. If dark matter distribution in the halo is favorable (in particular if it exhibits a sharp spike near the galactic center, or is highly clumped on short distance scales), ground-based telescopes such as VERITAS and HESS may also be able to observe a gamma-ray signal. In this case, it might also be possible to observe the monochromatic and the FSR components of the photon flux, whose spectra exhibit well-defined features (a line and an edge, respectively) and would provide smoking-gun evidence for the WIMP-related nature of the signal.

ACKNOWLEDGMENTS

We are grateful to Jay Hubisz and Patrick Meade for useful discussions. M. P., A. N. and A. S. are supported by the NSF grant No. PHY-0355005.

[1] For a recent review and a collection of references, see G. Bertone, D. Hooper, and J. Silk, Phys. Rep. **405**, 279 (2005).
[2] N. Arkani-Hamed, A. G. Cohen, E. Katz, and A. E. Nelson, J. High Energy Phys. 07 (2002) 034.
[3] M. Schmaltz and D. Tucker-Smith, hep-ph/0502182.
[4] M. Perelstein, hep-ph/0512128.
[5] S. Chang and H. J. He, Phys. Lett. B **586**, 95 (2004).
[6] G. Burdman, M. Perelstein, and A. Pierce, Phys. Rev. Lett. **90**, 241802 (2003); **92**, 049903(E) (2004); T. Han, H. E. Logan, B. McElrath, and L. T. Wang, Phys. Rev. D **67**, 095004 (2003); M. Perelstein, M. E. Peskin, and A. Pierce, Phys. Rev. D **69**, 075002 (2004).
[7] C. Csaki, J. Hubisz, G. D. Kribs, P. Meade, and J. Terning, Phys. Rev. D **67**, 115002 (2003); J. L. Hewett, F. J. Petriello, and T. G. Rizzo, J. High Energy Phys. 10 (2003) 062.
[8] H. C. Cheng and I. Low, J. High Energy Phys. 09 (2003) 051; 08 (2004) 061.
[9] I. Low, J. High Energy Phys. 10 (2004) 067.
[10] J. Hubisz, P. Meade, A. Noble, and M. Perelstein, J. High Energy Phys. 01 (2006) 135.
[11] J. Hubisz and P. Meade, Phys. Rev. D **71**, 035016 (2005).See also Phys. Rev. D **71**, 035016 (2005); note, however, that the dark matter relic density plot has not been updated in the journal version.
[12] D. E. Kaplan and M. Schmaltz, J. High Energy Phys. 10 (2003) 039; M. Schmaltz, J. High Energy Phys. 08 (2004) 056.
[13] A. Martin, hep-ph/0602206.
[14] A. Birkedal-Hansen and J. G. Wacker, Phys. Rev. D **69**, 065022 (2004).
[15] J. Hubisz, S. J. Lee, and G. Paz, hep-ph/0512169.
[16] H. C. Cheng, I. Low, and L. T. Wang, hep-ph/0510225.

[17] A. Birkedal, K. Matchev, and M. Perelstein, Phys. Rev. D **70**, 077701 (2004).
[18] G. Servant and T. M. P. Tait, Nucl. Phys. **B650**, 391 (2003).
[19] H. C. Cheng, J. L. Feng, and K. T. Matchev, Phys. Rev. Lett. **89**, 211301 (2002).
[20] D. N. Spergel *et al.* (WMAP Collaboration), Astrophys. J. Suppl. Ser. **148**, 175 (2003).
[21] A. Pukhov, hep-ph/0412191.
[22] G. Belanger, F. Boudjema, A. Pukhov, and A. Semenov, hep-ph/0405253.
[23] B. C. Allanach *et al.*, hep-ph/0602198.
[24] G. Belanger, F. Boudjema, A. Pukhov, and A. Semenov, hep-ph/0607059; the code can be obtained from ihttp://lappweb.in2p3.fr/lapth/micromegas/.
[25] R. J. Scherrer and M. S. Turner, Phys. Rev. D **33**, 1585 (1986); **34**, 3263(E) (1986).
[26] L. B. Okun, *Leptons and Quarks* (1982), pp. 228–231.
[27] G. K. Mallot, in *Proc. of the 19th Intl. Symp. on Photon and Lepton Interactions at High Energy LP99*, edited by J. A. Jaros and M. E. Peskin [Int. J. Mod. Phys. A 15S1, 521 (2000) eConf C990809, 521 (2000).
[28] D. S. Akerib *et al.* (CDMS Collaboration), Phys. Rev. Lett. **96**, 011302 (2006).
[29] SuperCDMS (Projected) Phase C [from the Dark Matter Plotter web site, http://dmtools.berkeley.edu/limitplots/].
[30] G. J. Alner *et al.* (UK Dark Matter Collaboration), Phys. Lett. B **616**, 17 (2005).
[31] N. J. C. Spooner *et al.*, Phys. Lett. B **473**, 330 (2000).
[32] M. Asano, S. Matsumoto, N. Okada, and Y. Okada, hep-ph/0602157.
[33] L. Bergstrom and P. Ullio, Nucl. Phys. **B504**, 27 (1997); Z. Bern, P. Gondolo, and M. Perelstein, Phys. Lett. B **411**, 86 (1997).
[34] M. A. Shifman, A. I. Vainshtein, M. B. Voloshin, and V. I. Zakharov, Yad. Fiz. **30**, 1368 (1979) [Sov. J. Nucl. Phys. **30**, 711 (1979)].
[35] J. F. Gunion, H. E. Haber, G. L. Kane, and S. Dawson, *The Higgs Hunter's Guide* (Perseus, Cambridge, MA, 1990); see also hep-ph/9302272.
[36] T. Han, H. E. Logan, B. McElrath, and L. T. Wang, Phys. Lett. B **563**, 191 (2003); **603**, 257(E) (2004).
[37] C. R. Chen, K. Tobe, and C. P. Yuan, hep-ph/0602211.
[38] L. Bergstrom, P. Ullio, and J. H. Buckley, Astropart. Phys. **9**, 137 (1998).
[39] K. Kosack *et al.* (VERITAS Collaboration), Astrophys. J. **608**, L97 (2004); K. Tsuchiya *et al.* (CANGAROO-II Collaboration), Astrophys. J. **606**, L115 (2004); F. Aharonian *et al.* (HESS Collaboration), Astron. Astrophys. **425**, L13 (2004).
[40] J. F. Navarro, C. S. Frenk, and S. D. M. White, Astrophys. J. **490**, 493 (1997).
[41] B. Moore, F. Governato, T. Quinn, J. Stadel, and G. Lake, Astrophys. J. **499**, L5 (1998); B. Moore, T. Quinn, F. Governato, J. Stadel, and G. Lake, Mon. Not. R. Astron. Soc. **310**, 1147 (1999).
[42] G. R. Blumenthal, S. M. Faber, R. Flores, and J. R. Primack, Astrophys. J. **301**, 27 (1986); F. Prada, A. Klypin, J. Flix, M. Martinez, and E. Simonneau, astro-ph/0401512; O. Y. Gnedin, A. V. Kravtsov, A. A. Klypin, and D. Nagai, Astrophys. J. **616**, 16 (2004).
[43] T. C. Weekes *et al.*, Astropart. Phys. **17**, 221 (2002).
[44] J. A. Hinton (HESS Collaboration), New Astron. Rev. **48**, 331 (2004).
[45] A. Morselli, A. Lionetto, A. Cesarini, F. Fucito, and P. Ullio (GLAST Collaboration), Nucl. Phys. B, Proc. Suppl. **113**, 213 (2002).
[46] T. Sjostrand, S. Mrenna, and P. Skands, J. High Energy Phys. 05 (2006) 026.
[47] A. Birkedal, K. T. Matchev, M. Perelstein, and A. Spray, hep-ph/0507194.
[48] L. Bergstrom, T. Bringmann, M. Eriksson, and M. Gustafsson, Phys. Rev. Lett. **95**, 241301 (2005).